

High Thermopower and Optical Properties of A_2MoS_4 ($A = K, Rb, Cs$) and Cs_2MoSe_4

Argha Jyoti Roy, Vineet Kumar Sharma, and Venkatakrishanan Kanchana*

The current work analyzes the electronic, structural, mechanical, thermoelectric (TE), and optical properties of alkali-based transition metal chalcogenides A_2MoS_4 ($A = K, Rb, Cs$) and Cs_2MoSe_4 using methods based on first principles. The electronic, structural, and mechanical properties are analyzed using projected augmented wave (PAW) potentials. The electronic structure calculations show them to be direct bandgap semiconductors. From the TE properties, it is found that all the compounds possess huge thermopower especially for the holes, and this along with low lattice thermal conductivity enables us to predict A_2MoS_4 ($A = K, Rb, Cs$) and Cs_2MoSe_4 to be a good class of material for TE applications. Also, the optical properties are found to be nearly isotropic in the low energy region, which also might fetch potential applications in the visible range. The nearly isotropic optical properties along with giant thermopower are the highlights of the current study, which sets a platform for exploring future device applications.

1. Introduction

The alarming increase in the rate of fossil fuel's consumption is a major concern around the globe. Almost two-thirds of fossil fuel energy is wasted in the form of heat energy^[1] and the depletion of fuels has pushed humanity to look for cleaner and much more efficient alternatives. Among all the viable options of renewable energy such as biomass, solar power, wind energy, geothermal energy, and so on, thermoelectricity emerges as an option. Thermoelectric (TE) materials not only can convert the waste heat energy into electrical energy but can also be used for power generation, refrigeration, and energy conservation. Due to the ability of electrons to conduct heat and transfer charge, TE materials are of great interest. The aptness of the TE materials is determined by a dimensionless quantity figure of merit $ZT = S^2\sigma T/\kappa$, where S is the Seebeck coefficient, σ is the electrical conductivity, κ is the thermal conductivity, and T being the absolute temperature. Due to the conflicting nature of S and σ , there is a compromise between the effective mass and carrier concentration and this makes difficulty in selecting the right materials.

A. J. Roy, V. K. Sharma, Dr. V. Kanchana
Department of Physics
Indian Institute of Technology Hyderabad
Kandi, 502285 Sangareddy, Telangana, India
E-mail: kanchana@iith.ac.in

 The ORCID identification number(s) for the author(s) of this article can be found under <https://doi.org/10.1002/pssb.202000587>.

DOI: 10.1002/pssb.202000587

From the empirical relation of ZT , it is well understood that κ must be low, which is contributed by both the electrons κ_e and the phonons κ_l . The electrical part of thermal conductivity is given by Wiedemann–Franz law ($\kappa_e = L\sigma T$) where L is the Lorenz number and therefore tuning this can affect σ , whereas lattice thermal conductivity $\kappa_l = \frac{1}{3}v_l C_v$ is independent of electronic interaction because κ_l , importantly enough, is dominated by phonon–phonon-scattering according to Keyes' expression^[2] and lowering it can significantly increase the ZT . If looked closely, ZT depends upon the parameters such as degeneracy of band extrema and a presence of it increases ZT ^[3] because the total power factor is a summation over all such extrema.^[4,5] Similarly, it depends

upon the effective mass anisotropy, which for high ZT value must be high.^[3]

Chalcogen-based compounds are a good candidate for TE purposes, and research over the years has suggested the same. Sankar et al.^[6] reported the Seebeck coefficient of $Tl_2PbHfSe_4$ to be 420 $\mu V/K$ at 520 K; high ZT of 1.4 for bulk chalcopyrite $CuGaTe_2$ was reported by Plirdpring et al.,^[7] whereas a theoretical calculation shows the ZT to be 1.65 at 950 K at hole concentration $3.7 \times 10^{19} \text{ cm}^{-3}$ ^[8]. Reported by Venkatasubramanian et al.,^[9] p-type Bi_2Te_3/Sb_2Te_3 superlattices have exhibited a ZT of 2.4 at 300 K. Chalcogenides also form complex crystal structures that result in low thermal conductivity as was in the case of Cu_3SbX_4 .^[10] Furthermore, there has been an enhancement of TE properties reported such as a high ZT of 1.5 at 773 K in Tl-doped p-type PbTe due to distortion in electronic density of states (DOS) through resonant impurities.^[11] Due to Sn doping there is a significant enhancement in the value of the thermopower of Bi_2Te_3 single crystal as Sn offers resonant states enhancing the DOS near the Fermi level.^[12] As stated earlier, the reduction of κ_l also can enhance TE properties. The reduction occurs by an increase in phonon–phonon-scattering near the grain boundaries, structural defect, and interfaces in the nanostructured materials. For example, optimization of nanostructures to reduce κ_l produces a ZT of 1.8 achieved in the Na-doped PbTe at 800 K reported by Girard et al.^[13] A whopping ZT value of 2.6, as reported by Zhao et al.,^[14] was obtained in the undoped monocrystalline SnSe at 923 K with the ultralow intrinsic κ_l of the crystal. The heavy atomic weight of the chalcogens is also beneficial for reducing lattice thermal conductivity in the materials.^[10]

The classification of the materials for optical applications is determined by the bandgap and therefore electronic structure. Chalcogen-based materials find their suitability in all kind of fields such as solar cell, optoelectronic, photovoltaic, and so on. Compounds such as Cu_2GeSe_4 , as reported by Choi et al.,^[15] are found to have potential applications in optics. Layered oxychalcogenides such as LaCuOCh ($\text{Ch} = \text{S}, \text{Se}, \text{and Te}$)^[16] find its application in the field of optoelectronics. Diamond-like quaternary semiconductors $\text{CuMn}_2\text{InSe}_4$ ^[17] are multiversatile compounds having huge range of field of applications. Other quaternary chalcogen compounds $\text{Cu}_2\text{ZnSnX}_4$ have potential application in optoelectronic devices,^[18] photovoltaic absorbers,^[19] and as a TE material.^[20]

The transition metal dichalcogenides MoS_2 , MoSe_2 , and WSe_2 are rich in terms of physics and their utilities which span a major part of technology such as catalytic activity^[21] and photochemical process.^[22] The 2D structure of these compounds gained attention in photovoltaics,^[23] molecular sensing,^[24] photoluminescence,^[25,26] and nanoscale field-effective transistor.^[27,28] The monolayer of MoSe_2 is suitable for single-junction solar cell, photochemical cells,^[29] and can be tuned to have magnetic properties by doping of nonmetals with odd number of valence electrons.^[30] Another chalcogen-based material $\text{Cu}_2\text{CdSnSe}_4$ having 2:1:1:4 ratio shows enhanced TE properties with Mn doping on Cd sites.^[31] The earlier studies on the transition metal dichalcogenides together with other efficient chalcogen-based TE materials served as a motivation for us to explore this domain further in the realm of ab initio studies, and we have opted another series of chalcogenides in combination of alkali atoms with Mo atom. The current study is a complete analysis of structural, electronic, TE, and optical properties of A_2MoS_4 and Cs_2MoSe_4 . This article is organized in the following manner: Section 2 gives the methodology used followed by the results and discussions in Section 2 and finally Section 4 concludes the study.

2. Computational Details

Geometry optimization for all the investigated compounds has been conducted using the pseudopotential method as implemented in Vienna Ab Initio Simulation (VASP) package.^[32–35] PBEsol,^[36] a modified version of generalized gradient approximation under the parametrization of Perdew–Burke–Ernzerhof,^[37] has been used for exchange correlation functional. The tetrahedron method is being used to integrate Brillouin zone (BZ).^[38] The energy cutoff is set to 520 eV. The energy convergence and force tolerance are 10^{-6} Ry and 10^{-2} eV \AA^{-1} . A finite difference method implemented in VASP code is used to calculate elastic tensor. A k -point sampling is done using a mesh of $13 \times 8 \times 7$ in the irreducible BZ within Monkhorst Pack scheme.^[39] Ground-state properties of all the compounds are obtained after it reaches self-consistency with energy convergence of 10^{-6} Ry. The Bader charge analysis is also being done to compute the charge transfer among atoms using a combination of VASP and postprocessing VASP utility Bader.^[40–43] The TE coefficients such as thermopower and electrical conductivity are being calculated using the Boltzmann transport theory implemented in BoltzTraP code.^[44] Two approximations, such as the constant scattering time approximation (CSTA) and another one rigid band

approximation (RBA),^[45–47] have been used to calculate the near-equilibrium TE coefficients. The static part of optical properties has been computed using VASP. A postprocessing tool VASPKIT^[48] has been used to extract the optical properties using VASP outputs.

3. Results and Discussion

3.1. Structural Properties

The investigated compounds A_2MoS_4 ($\text{A} = \text{K}, \text{Rb}, \text{Cs}$) and Cs_2MoSe_4 are built of $[\text{MoX}_4]^{2-}$ ($\text{X} = \text{S}, \text{Se}$) cluster and A^+ ions crystallizing in an orthorhombic structure with space group $Pnma$ (62) having four formula units.^[49–52] In particular, Cs_2MoS_4 and Rb_2MoS_4 are a derivative of the structure of $\beta\text{-K}_2\text{SO}_4$ ^[53] and $(\text{NH}_4)_2\text{MoS}_4$ ^[54] and K_2MoS_4 is isostructural to Cs_2MoS_4 and Rb_2MoS_4 .^[49] The crystal structure is shown in **Figure 1**.

Table 1 shows the comparison between the theoretically calculated and experimentally reported lattice parameters. Our calculated optimized results are in good accordance with the experimental values.

Elastic constants are fundamental properties of any crystalline material which describe the resistance of the material when undergoes mechanical pressure, strain, and so on. This also signifies the stability of the materials. The investigated compounds crystallize in an orthorhombic structure which has nine independent elastic components, namely, $C_{11}, C_{22}, C_{33}, C_{44}, C_{55}, C_{66}, C_{12}, C_{13}, \text{and } C_{23}$. These are calculated at a constant theoretical volume as shown in **Table 2** and are found to satisfy Born criteria of mechanical stability for orthorhombic structure as given in the previous study.^[55] Using these single-crystal elastic constants, we also calculated polycrystalline aggregate properties such as bulk ($B_X, X = V, R, \text{and } H$) and shear moduli ($G_X, X = V, R, \text{and } H$) under Voigt,^[56] Reuss,^[57] and Voigt–Reuss–Hill^[58] approximation. Furthermore, we also computed Debye temperature (Θ_D) which is a fundamental quantity of any material as it is linked to specific heat, thermal conductivity. From the low values of the elastic constants, Young modulus, and Bulk modulus, we can conclude that both the systems have less resistance to used strain, pressure, and so on, and could be resulted in a structural transition at an intermediate pressure value. The pressure

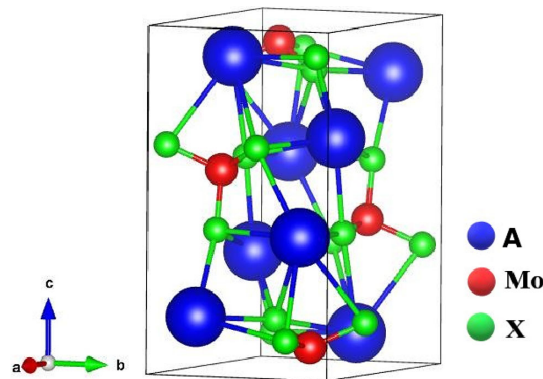


Figure 1. Crystal structure of A_2MoS_4 and Cs_2MoSe_4 .

Table 1. Calculated lattice parameters of A_2MoS_4 ($A = K, Rb, Cs$) and Cs_2MoSe_4 along with the experimental values.

Compounds	K_2MoS_4		Rb_2MoS_4		Cs_2MoS_4		Cs_2MoSe_4	
	Theo.	Exp.	Theo.	Exp.	Theo.	Exp. (27)	Theo.	Exp.
a [Å]	9.35	9.32	9.66	9.65	10.05	10.04	10.40	10.33
b [Å]	6.74	6.84	6.91	7.03	7.12	7.24	7.35	7.47
c [Å]	12.00	12.08	12.27	12.43	12.62	12.78	12.90	13.06

Table 2. Calculated elastic constants C_{ij} , Young's modulus (GPa), bulk modulus (GPa), velocities of sound (ν_l, ν_t, ν_{mean} ; in $km\ s^{-1}$), and Debye temperature (Θ_D in K).

Elastic constants	K_2MoS_4	Rb_2MoS_4	Cs_2MoS_4	Cs_2MoSe_4
C_{11}	29.6	25.52	22.09	19.32
C_{22}	35.0	32.43	31.23	29.63
C_{33}	29.8	25.43	21.86	23.09
C_{44}	6.82	7.41	7.49	6.46
C_{55}	5.88	6.85	6.54	5.37
C_{66}	8.66	8.97	8.13	7.18
C_{12}	8.35	8.11	8.778	7.10
C_{13}	10.62	9.38	8.57	8.28
C_{23}	6.60	6.80	7.72	6.86
E_H	21.76	21.23	19.41	17.66
B_H	16.19	14.62	13.77	12.82
G_H	8.53	8.43	7.67	6.95
ν_l	3.22	2.84	2.58	2.20
ν_t	1.78	1.62	1.45	1.23
ν_{mean}	1.99	1.80	1.62	1.37
Θ_D	198.18	174.30	151.83	124.80

studies on the compound Cs_2MoS_4 have been reported earlier by Lorenz et al.^[59] which suggests two structural phase transition at 8 and 9.7 GPa due to phonon-softening. The Debye temperature is an essential parameter for every material as it signifies the temperature of the normal mode of vibration of the lattice. Essentially, the value of Θ_D plays an important role in thermodynamic and thermal properties such as phonons, specific heat, and thermal expansion.^[60] $\Theta_D \approx \sqrt{Y/M}$, which signifies the relation of Debye's temperature and elastic properties. Θ_D is also connected to lattice thermal conductivity also, which is an integral part for any TE materials. A higher value of Θ_D suggests high κ_l , but for our investigated compound it turned out to be low as shown in Table 2, which indicates the compounds to possess low thermal conductivity and which checks out with the calculated κ_l , presented in a later section.

3.2. Electronic Structure Properties

Using the optimized lattice parameters, the electronic structure and transport properties have been computed. The electronic properties were calculated using PBEsol XC functional. The band plot of K_2MoS_4 is shown in Figure 2a. The band plot for

remaining compounds is shown in Figure S1, Supporting Information. It is evident from the band structure that the compounds are direct bandgap semiconductors with gap of 1.19, 1.30, 1.64, and 1.07 eV for A_2MoS_4 ($A = K, Rb, Cs$) and Cs_2MoSe_4 , respectively. Evidently, there is an increase in the bandgap as we move from K to Cs, and this behavior of the bandgap suggests that the alkali atoms play almost no role near the Fermi level and are not the key players for TE aspects, whereas in case of Cs_2MoSe_4 and Cs_2MoS_4 we observe a decrease in the bandgap, which is expected as we go down the column of elements in the periodic table. These details can be observed in the DOS plots as shown in Figure 2b,c. The profile of the bands is important for our case as it is tied to the effective mass of the charge carriers. The effective mass is an essential quantity for TE materials. Effective mass is inversely proportional to the curvature of the bands which is nothing but the second-order derivative of band dispersion.^[61] The profile of the bands is almost the same for all the investigated compounds. Along the three crystallographic directions, the dispersion of bands in the conduction band region is very much alike in all the investigated compounds.

Also, the dispersive nature of the conduction band is quite prominent and hence an indication to smaller effective mass m^* . In case of valence band along Γ -X direction, we observe flat bands implying high effective mass of the charge carriers compared with other crystallographic direction. This also indicates that thermopower for holes will be higher than the electrons. As a part of this work is focused on TE properties of A_2MoX_4 and Cs_2MoSe_4 , calculating effective mass is a necessity to extract the TE coefficients. We have calculated the effective masses of concerned compound in different crystallographic direction in BZ and the same is shown in Table 3.

To analyze more about the electronic structure, a knowledge of DOS is important for both the compounds and is shown in Figure 2b,c. For both the compounds, we observe narrow deep lying states centered around -7.5 to -8 eV below the Fermi level, which are due to the alkali p orbital. Bit closer to the Fermi level, we observe hybridized states between chalcogen p and Mo d orbital. In the close proximity of the Fermi level in the valence band region, the p orbital of the chalcogen dominates. In the conduction band region, the unoccupied states near the Fermi level have large contribution from Mo d orbital; deep within the conduction band the states are due to again alkali atom. The behavior of the bandgap observed can also be explained by the DOS. For the alkali series, all the alkali atoms contribute to deep lying states and moving from K to Cs the gap increases. In case of Cs_2MoSe_4 and Cs_2MoS_4 , the chalcogen atom contributes near the Fermi level and therefore moving from S to Se more states become available and therefore the gap decreases.

Furthermore, the insight to contribution of atoms near Fermi level is an important one because this can be utilized in selecting dopant that can enhance the TE properties.

To understand the nature of bonding, the charge density is being plotted along (010) plane as shown in Figure 2d for K_2MoS_4 . The charge density plots for other compounds are shown in Figure S2, Supporting Information.

From the plots, it is observed that there is covalent bonding between the transition metal Mo and chalcogen atoms. Due to the high electronegativity ($K = 0.82$; $Rb = 0.82$; $Cs = 0.79$;

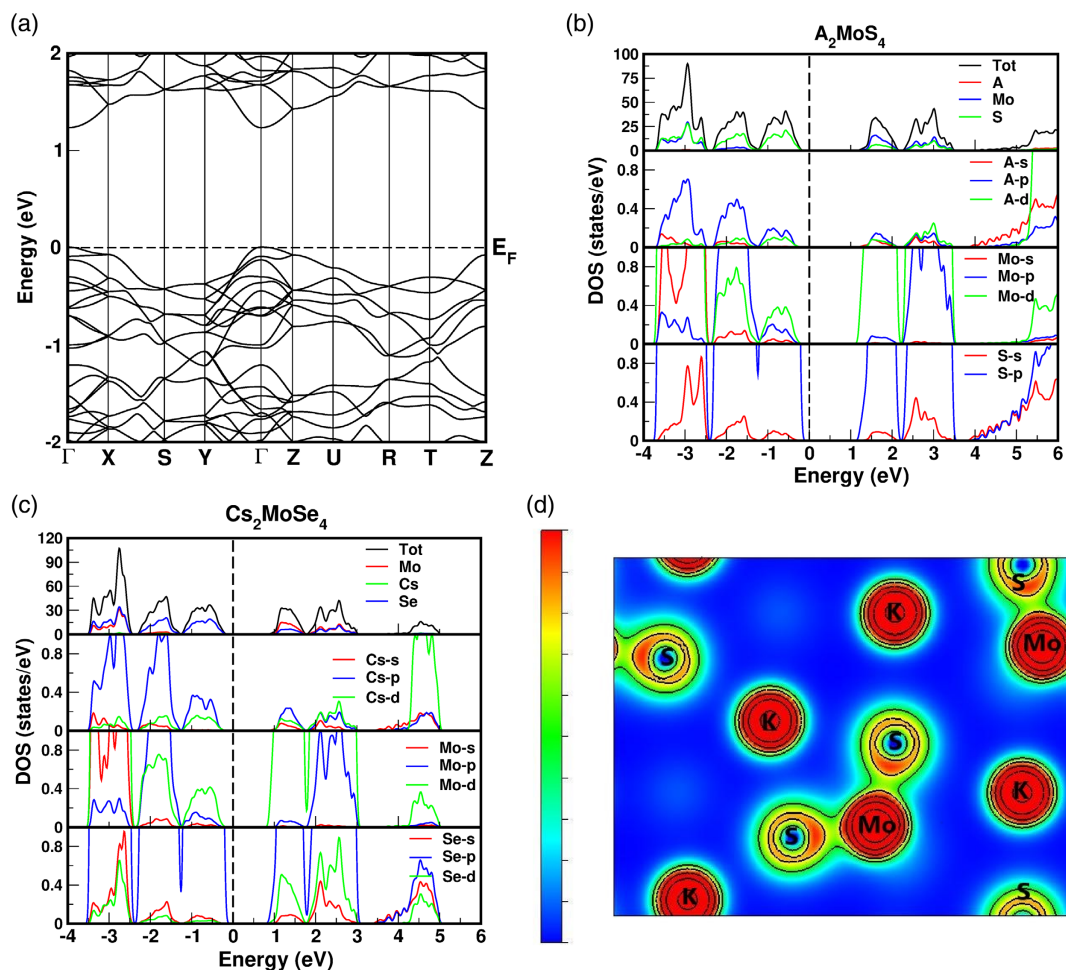


Figure 2. a) Band structure of K_2MoS_4 , the DOS of b) A_2MoS_4 and c) Cs_2MoSe_4 , and d) the charge density of K_2MoS_4 along (010) plane.

Table 3. Calculated effective masses of A_2MoS_4 ($A = K, Rb, Cs$) and Cs_2MoSe_4 along crystallographic directions of the BZ.

Direction	K_2MoS_4		Rb_2MoS_4		Cs_2MoS_4		Cs_2MoSe_4	
	$M_h(m_e)$	$M_e(m_e)$	$M_h(m_e)$	$M_e(m_e)$	$M_h(m_e)$	$M_e(m_e)$	$M_h(m_e)$	$M_e(m_e)$
$\Gamma-X$	1.61	0.16	1.40	0.17	1.80	0.17	1.47	0.15
$\Gamma-Y$	0.19	0.14	0.25	0.14	0.82	0.10	0.27	0.13
$\Gamma-Z$	0.31	0.13	0.32	0.15	0.31	0.18	0.28	0.14

Mo = 2.16; S = 2.58; Se = 2.55) difference between the alkali and the other atoms, it forms an ionic bond with rest of them, whereas the electronegativity difference between them is small and therefore the covalent nature can be seen between them. To get more details about the charge transfer, we have also calculated the average charge per atom of the investigated compounds shown in Table 4. The number of electrons contributing to pseudopotential used for our calculations is 9, 12, and 6 for alkali, Mo, and chalcogens, respectively. The electronegativity of chalcogens is higher as compared with alkali and Mo atom as discussed earlier. This nature is reflecting in the values of average charge per atom in Table 4. The chalcogens are gaining the charge, while the alkalis and Mo atom are losing it.

The net charge lost by alkali and Mo atoms is same as the net charge gained by chalcogens which is a sign of ionic bonding.

The importance of bonding linked with other physical properties of a material is explained here. The observed high ionicity between the alkali atoms and the rest of them in all the compounds could be the reason for exhibiting low elastic constants which might drive structural transition. Covalent bonding between Mo and chalcogen atoms may contribute to lighter charge carriers as the effective mass is inversely proportional to the overlap integral of the orbitals. Similarly, ionic nature of alkali atom provides very less overlap, leading to higher effective mass of charge carriers. Lighter bands favoring high mobility together with heavier bands leading to higher thermopower may

Table 4. Bader charge calculated for the compounds. Here, A is being used for corresponding alkali atom.

Av. atomic charge per atom	K ₂ MoS ₄	Rb ₂ MoS ₄	Cs ₂ MoS ₄	Cs ₂ MoSe ₄
A(1)	8.189	8.193	8.204	8.190
A(2)	8.171	8.176	8.234	8.207
Mo	10.643	10.650	10.632	10.941
S(1)	6.797	6.759	6.748	–
S(2)	6.736	6.756	6.755	–
S(3)	6.701	6.718	6.724	–
S(4)	6.762	6.744	6.743	–
Se(1)	–	–	–	6.656
Se(2)	–	–	–	6.795
Se(3)	–	–	–	6.640
Se(4)	–	–	–	6.640

project these compounds as good thermoelectric material which is discussed in the upcoming section.

3.3. TE Properties

In this section, we will discuss the TE properties of the investigated compounds. We have utilized Boltzmann transport theory as implemented in BoltzTrap^[44] code to compute the TE properties of the compounds. Here, we have computed thermopower ($\mu\text{V}/\text{K}$), electrical conductivity scaled by relaxation time ($\Omega^{-1}\text{m}^{-1}\text{s}^{-1}$) and power factor scaled by relaxation time ($\text{W mK}^{-2}\text{s}^{-1}$). The probed compound is orthorhombic and we have computed TE properties along the three crystallographic directions as a function of electron and hole concentration as shown in **Figure 3** and **4** for K₂MoS₄. It is important to consider the directional dependence of the TE properties as it reveals the anisotropy in the system^[8,14,62] which was observed in PdCoO₂ and PtCoO₂ where a large difference between in-plane and out-of-plane TE properties was noted.^[62]

The thermopower is a measure of asymmetry in band structure and scattering rates near the Fermi level^[3] and the same is shown in **Figure 4a** and **Figure 5a** and **Figure S3a–S8a**, Supporting Information. The thermopower for holes is found to be higher than electrons throughout the whole temperature range. The difference between the thermopower of holes and electrons is about 100–200 $\mu\text{V K}^{-1}$. The thermopower for holes of A₂MoS₄ (A = Cs, Rb, K) at 300 K is nearly 720, 610, and 580 $\mu\text{V K}^{-1}$, respectively, and for Cs₂MoSe₄ derivative, it is 600 $\mu\text{V K}^{-1}$. It reaches a maximum value of 800 $\mu\text{V K}^{-1}$ at 700 K for Cs₂MoS₄. For the electrons, the thermopower is mostly within 650 $\mu\text{V K}^{-1}$ at 300 K for all the compounds and reaches a maximum value of nearly 680 $\mu\text{V K}^{-1}$ at 700 K for Cs₂MoS₄.

The comparative study with well-known TE materials is reported earlier such as Bi₂Te₃, which has thermopower of 225 $\mu\text{V K}^{-1}$ at room temperature^[6,63] Tl₂PbHfSe₄ which possesses thermopower around 420 $\mu\text{V K}^{-1}$ at 520 K, and a thermopower value of nearly 600 $\mu\text{V K}^{-1}$ for CuGaTe₂^[8] emphasizes that thermopower is huge in our case, and it indicates that the

investigated system can fetch application in power generation. Some other previous works on TEs such as olivine-type Fe₂GeCh₄ (Ch = S, Se, Te)^[64] and OsX₂ (X = S, Se, Te)^[65] which have the same group elements as our investigated compounds are found to have a thermopower of 600–800 $\mu\text{V K}^{-1}$ for hole doping which supports the current study. We also observe an anisotropy along *a*-axis in case of holes, which is due to the occurrence of a flat valence band along Γ –X direction meaning high effective mass. Contrastingly, we find almost isotropic thermopower for electrons along the crystallographic directions. Though a very small anisotropy exists in case of Cs₂MoS₄, it should also be noted that the thermopower for electrons is also quite high. As we move from K to Cs, the bandgap increases, which results in increase in thermopower. Also for S and Se derivative, Cs₂MoS₄ has high thermopower. Out of all the investigated compounds, p-type K₂MoS₄ has greater thermopower.

Along with the thermopower, we have also calculated electrical conductivity scaled by relaxation time (σ/τ) and are shown in **Figure 4b** and **5b** and **Figure S3b–S8b**, Supporting Information. All the compounds have a higher value of electrical conductivity along the *b*-axis. We observe large anisotropy in the case of holes. We observe high dispersion along Γ –Y which might be due to the covalent bonding between Mo–X (X = S, Se), resulting in a low effective mass and therefore higher value of electrical conductivity. In the case of electrons, the observed anisotropy along the crystallographic direction is lesser than the holes.

We have calculated one of the important transport properties called mobility scaled by relaxation time along all the three crystallographic directions. The mobility of any material evaluates its transfer efficiency. Mobility as a function of carrier concentration is shown in **Figure 3d** and **4d** for K₂MoS₄. The mobility plots for other three compounds are shown in **Figure S9**, Supporting Information. From the plots, it is observed that the mobility is carrier independent for a long range of carrier concentration ranging from 10¹⁸ to 10²⁰ cm^{–3}. The order of mobility for both carriers is almost the same. The anisotropy can also be seen in carrier mobility especially for holes in all the compounds. The similar order of mobility for both carriers along with anisotropic nature infers that both types of carriers are suitable for device applications, and holes are more favorable.

Furthermore, we have calculated the power factor presented in **Figure 4c**, and **5c**. The power factor for other compounds is shown in **Figure S3c–S8c**, Supporting Information. The power factor is a combined effect of both thermopower and the electrical conductivity scaled by relaxation time. For all the compounds, the power factor along *b*-axis is higher due to the higher value of σ/τ along that direction. From the plots, it can be seen that power factor for holes A₂MoS₄ is higher than electron, whereas Cs₂MoS₄ has high power factor than Cs₂MoSe₄. We observe anisotropy along the crystallographic direction for concentration ranges from 10¹⁸ to 10¹⁹. The anisotropy is increasing as a function of both carrier concentration and temperature. However, we can say that all the compounds favor hole doping for TE properties, but the contribution to TE properties for electron doping is also good.

Unfortunately, there are no reported data available for the TE properties of these compounds and therefore our calculations await experimental confirmations.

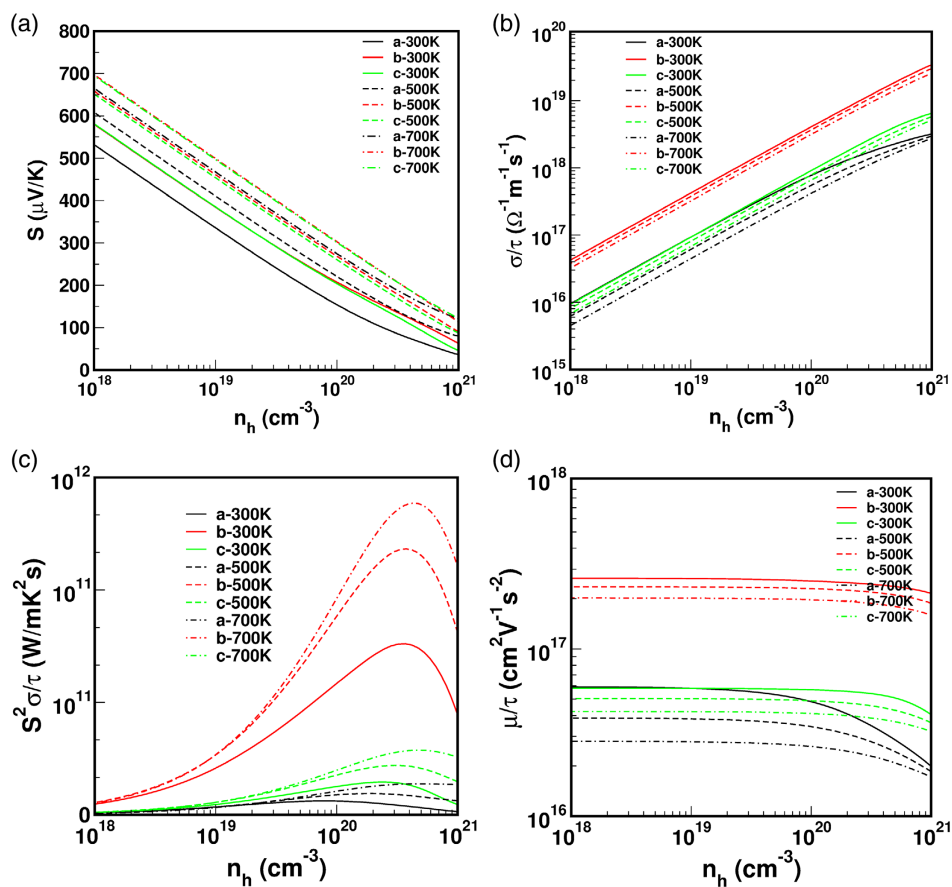


Figure 3. TE properties of K_2MoS_4 for holes: a) thermopower and b) electrical conductivity, c) power factor and d) mobility scaled by relaxation time.

3.4. Thermal Conductivity

Lattice thermal conductivity hugely depends on the lattice vibrations, more precisely on the elastic constants of the system. More importantly, the acoustic phonon-modes play a major part in heat transfer in semiconductors.^[66] The anharmonicity^[67] in system also lowers the value of κ_1 as observed in $AgSbTe_2$ ^[68–70] Cu_2SbSe_3 , $SnSe$ ^[14] and so on. The strong phonon–phonon-scattering will limit the value of mean free path and therefore reducing the lattice thermal conductivity.^[71,72] For the investigated compounds, we have used Cahill’s model^[73] to estimate the order of thermal conductivity, as shown in Table 5. We observe a decrease in the value of κ_1 as we move from K to Cs and attain the lowest value for Cs_2MoSe_4 . For all the investigated compounds, we find small values of elastic properties but K_2MoS_4 having the highest and Cs_2MoSe_4 having the lowest of all and this may be due to weak interatomic interactions that are reflected in the elastic properties.^[74] To get a better idea, first-principles quasiharmonic phonon-calculations are required, but a qualitative assessment can be given using Slack’s model^[66,75] of thermal conductivity. The model depends directly on the third power of Θ_D . Therefore, K_2MoS_4 will have higher thermal conductivity and Cs_2MoSe_4 will have lowest of the lot which is also seen in Table 5. Importantly enough κ_{min} for all the compounds

are less than unity and therefore these investigated compounds might be promising TE materials.

4. Optical Properties

Here, we report the optical properties of the investigated compound. Dielectric function $\epsilon(\omega)$ can be utilized to relate with a linear response of the electromagnetic radiation, i.e., describing the interaction between photon and electron. The optical transition mechanism is described by the imaginary part $\epsilon''(\omega)$. $\epsilon(\omega)$ has two contributions to its interband and intraband transitions.^[76] The intraband transitions are prominent for metals. Furthermore, interband transitions have two parts: direct and indirect transitions.^[77] The indirect optical transitions include phonon-scattering and have a small part in $\epsilon(\omega)$ ^[78] and therefore has been neglected here. The imaginary part of the dielectric constant is calculated using the empirical relation as given in the previous work,^[77] and the real part of the dielectric function is evaluated using the relation as reported in the earlier work.^[79]

The evaluation of the $\epsilon_R(\omega)$ requires good knowledge of $\epsilon_1(\omega)$ up to high energies. Here, we have calculated $\epsilon_1(\omega)$ till 50 eV and used this as truncated energy. Within this energy range, we have converged Kramers–Kronig transformation. To evaluate

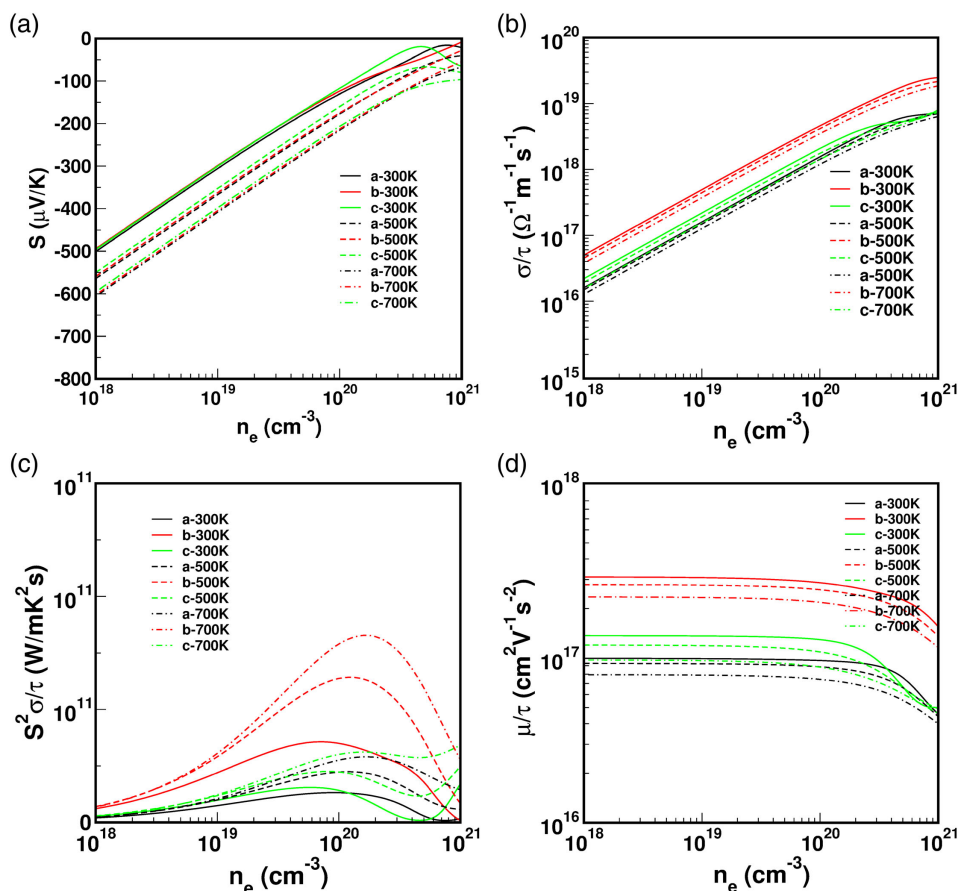


Figure 4. TE properties of K_2MoS_4 for electrons: a) thermopower and b) electrical conductivity, c) power factor and d) mobility scaled by relaxation time.

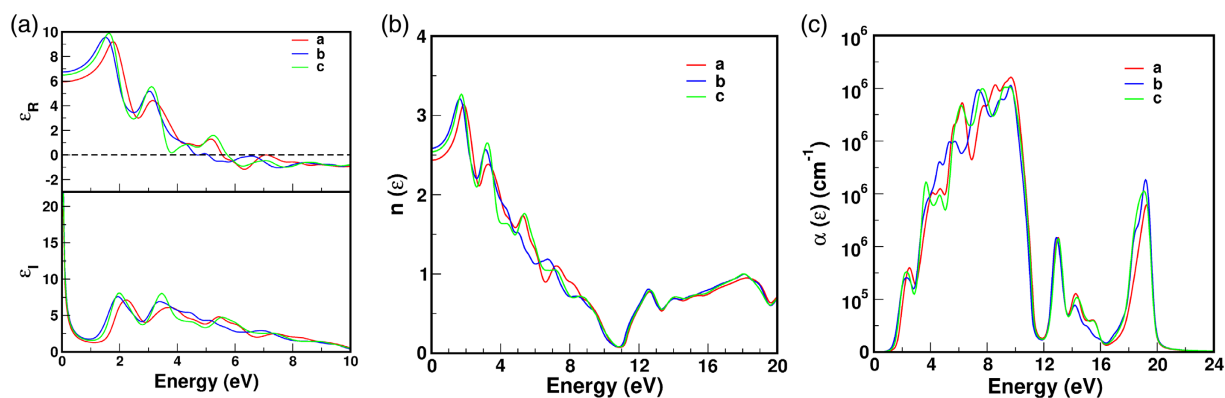


Figure 5. The optical properties of K_2MoS_4 : a) real and imaginary parts of the dielectric function, b) refractive index, and c) absorption spectra.

Table 5. Minimum thermal conductivity calculated for the compounds.

Compounds	κ_1 [$W m^{-1} K^{-1}$]
K_2MoS_4	0.41
Rb_2MoS_4	0.35
Cs_2MoS_4	0.30
Cs_2MoSe_4	0.24

important optical properties such as refractive index, reflectivity, and absorption coefficient, the knowledge of both ϵ_1 and ϵ_R is required. As the compounds are orthorhombic, the optical properties along the three axes are calculated. The imaginary part of $\epsilon(\omega)$ for all the compounds is found to have similar nature plotted in Figure 5a for K_2MoS_4 . The optical properties for the other compounds are shown in Figure S10–S12, Supporting Information.

For all the compounds, the anisotropy along the crystallographic axis is seen. The peaks for $\epsilon_1(\omega)$ are observed at 1.95, 3.47, and 5.44 eV for Ks_2MoS_4 and 2.03, 3.42, and 5.54 eV for Rbs_2MoS_4 (Figure S10a, Supporting Information), respectively, whereas the dominant peaks are observed at 2.16, 3.44, 4.51, and 5.50 eV for Cs_2MoS_4 (Figure S11a, Supporting Information) and 1.66, 2.98, 3.98, and 4.67 eV for Cs_2MoSe_4 (Figure S12a, Supporting Information), respectively. We observe the contents of the imaginary dielectric function to be shifted toward higher energy as we move from K to Cs, whereas shifting toward lower energy as we go down from S to Se derivative of Cs, and it can be related to band structure. It is important to identify these peaks occurring in ϵ_1 from our band structure calculations. We observe these peaks to occur due to the chalcogen *p*-states and 4 *d* states of Mo atom playing as initial and final states in the transitions. The real part of dielectric function ϵ_R is shown in Figure 5a for K_2MoS_4 . The behavior for A_2MoS_4 is very much similar to the contents shifted toward higher energy as we move from K to Cs. Almost three peaks are seen for all the compounds and about 4 eV parts of ϵ_R go below zero—till 6 eV. The negative values show the metallic behavior because zero absorption occurs in this range and the light is reflected.^[80] We observe considerable anisotropy along the three crystallographic axes in the ϵ_1 and ϵ_R spectra in the higher energy region. This anisotropy observed in the optical properties is a result of lower crystal symmetry and the band structure. The dielectric constant connects the optical and electronic properties. The strength of the interaction between the valence and conduction state in the presence of external electric field is given by polarization. For larger bandgap, the polarization is small, while small bandgap leads to easy polarization of the material and high value of dielectric constant. This explains the high value of $\epsilon_R(0)$ for K_2MoS_4 and Cs_2MoSe_4 than any other compound.

Next, we have calculated the refractive index which is similar to ϵ_R , which divides the light into its components along the three crystallographic directions, as shown in Figure 5b, for Ks_2MoS_4 . The nearly isotropic nature is found in a low energy regime which increases as the energy increases. The refractive index attains a maximum with the increasing energy and higher energy values start to decrease. At energy greater than 12 eV, the spectra are isotropic and fairly constant for all the compounds. The refractive index for A_2MoS_4 decreases as we move from K to Cs, whereas the refractive index increases from Cs_2MoS_4 (Figure S11b, Supporting Information) to Cs_2MoSe_4 (Figure S12b, Supporting Information) opposite of the bandgap. The static refractive index along the three crystallographic directions is shown in Table 6.

From the dielectric constants ϵ_R and ϵ_1 , we further calculated the absorption spectra as a function of photon energy is shown in

Table 6. The static refractive index of A_2MoS_4 and Cs_2MoSe_4 along all the crystallographic directions.

	K_2MoS_4	Rb_2MoS_4	Cs_2MoS_4	Cs_2MoSe_4
n_a	2.41	2.25	2.17	2.46
n_b	2.57	2.35	2.17	2.44
n_c	2.53	2.35	2.10	2.34

Figure 5c for K_2MoS_4 . The absorption spectra of the other compounds are shown in Figure (S10c, S11c, S12c, Supporting Information). The absorption spectra reveal the way materials absorb incident radiation. The absorption spectra can be connected to the electronic properties as it starts at the equivalent photon energy to the bandgap of all the compounds. Below this value, all are transparent. The peaks in absorption spectra characterize the transition between the states lying at the same energy interval. The first peak in all the compounds lies nearly around 2.5 eV. The anisotropy in the absorption spectra is less in the lower energy regime and is found to be increased with energy. The peaks lying in the higher energy region are evident for the same. The absorption spectra and isotropic nature in the refractive index reveal that the investigated compound can play a key role in device applications in nearly visible and UV regions. In addition, the value of refractive indices for the investigated systems lying between 2 and 3 along with direct bandgap might fetch optoelectronic applications.

5. Conclusion

The first-principles study of A_2MoS_4 and Cs_2MoSe_4 is done to explore their structural, mechanical, electronic, TE, and optical properties. The optimized parameters are in good agreement with the experimentally reported one. The electronic structure calculation shows the systems to have a direct bandgap. We have calculated TE properties as a function of carrier concentration. We observe very high thermopower for both charge carriers, but the hole contribution edges over slightly. From the absorption spectra, we observe the compound to be optically active in the visible and UV region. The carrier mobility is found to be almost same for the both carriers with significant anisotropy in the case of holes. The giant thermopower along with nearly isotropic nature in the refractive index opens up a channel for future device applications.

Supporting Information

Supporting Information is available from the Wiley Online Library or from the author.

Acknowledgements

The authors A.J.R., V.K.S., and V.K. would like to acknowledge IIT Hyderabad for providing the computational facilities. V.K.S. would like to acknowledge MHRD for fellowship. V.K. would like to acknowledge BRNS project with sanction no. (58/14/13/2019-BRNS).

Conflict of Interest

The authors declare no conflict of interest.

Data Availability Statement

Research data are not shared.

Keywords

computational physics, density functional theory, electronic structure, optical properties, thermoelectric materials, transport properties

Received: November 27, 2020

Revised: April 20, 2021

Published online:

- [1] J. He, M. G. Kanatzidis, V. P. Dravid, *Mater. Today* **2013**, *16*, 166.
- [2] R. W. Keyes, *Phys. Rev.* **1959**, *564*, 115.
- [3] J. Sootsman, D. Chung, M. Kanatzidis, *Angew. Chem. Int. Ed.* **2009**, *48*, 8616.
- [4] L. D. Hicks, M. S. Dresselhaus, *Phys. Rev. B* **1993**, *47*, 12727.
- [5] P. Larson, S. D. Mahanti, M. G. Kanatzidis, *Phys. Rev. B* **2000**, *61*, 8162.
- [6] C. R. Sankar, A. Assoud, H. Kleinke, *Inorg. Chem.* **2013**, *52*, 13869.
- [7] T. Plirdpring, K. Kurosaki, A. Kosuga, T. Day, S. Firdosy, V. Ravi, G. J. Snyder, A. Harnwungmoung, T. Sugahara, Y. Ohishi, H. Muta, S. Yamanaka, *Adv. Mater.* **2012**, *24*, 3622.
- [8] V. K. Gudelli, V. Kanchana, G. Vaitheeswaran, A. Svane, N. E. Christensen, *J. Appl. Phys.* **2013**, *114*, 223707.
- [9] R. Venkatasubramanian, E. Siivola, T. Colpitts, B. O'Quinn, *Nature* **2001**, *413*, 597.
- [10] H. Meng, M. An, T. Luo, N. Yang, in *Chalcogen: From 3D to 2D and Beyond* (Eds: X. Liu, S. Lee, K. J. Furdyna, T. Luo, H. Y. Zhang), Woodhead Elsevier, Cambridge, UK **2020**, pp. 44–45.
- [11] J. P. Heremans, V. Jovovic, E. S. Toberer, A. Saramat, K. Kurosaki, A. Charoenshakdee, S. Yamanaka, G. J. Snyder, *Science* **2013**, *321*, 554.
- [12] V. A. Kulbachinskii, V. G. Kytin, A. A. Kudryashov, R. A. Lunin, *J. Solid State Chem.* **2012**, *193*, 83.
- [13] S. N. Girard, J. He, X. Zhou, D. Shoemaker, C. M. Jaworski, C. Uher, V. P. Dravid, J. P. Heremans, M. G. Kanatzidis, *J. Am. Chem. Soc.* **2013**, *133*, 16588.
- [14] L.-D. Zhao, S.-H. Lo, Y. Zhang, H. Sun, G. Tan, C. Uher, C. Wolverton, V. P. Dravid, M. G. Kanatzidis, *Nature* **2014**, *508*, 373.
- [15] S. G. Choi, A. L. Donohue, G. Marcano, C. Rincón, L. M. Gedvilas, J. Li, G. E. Delgado, *J. Appl. Phys.* **2013**, *114*, 033531.
- [16] K. Ueda, H. Hiramatsu, M. Hirano, T. Kamiya, H. Hosono, *Thin Solid Films* **2006**, *496*, 15.
- [17] L. Salik, A. Bouhemadou, K. Boudiaf, F. S. Saoud, S. Bin-Omran, R. Khenata, Y. Al-Douri, A. H. Reshak, *J. Supercond. Novel Magn.* **2020**, *33*, 1091.
- [18] Y. Dong, P. Shen, X. Li, Y. Chen, L. Sun, P. Yang, J. Chu, *Mater. Res. Express* **2016**, *3*, 116411.
- [19] S. Chen, X. G. Gong, A. Walsh, S.-H. Wei, *Appl. Phys. Lett.* **2009**, *94*, 041903.
- [20] C. Sevik, T. Çağın, *Appl. Phys. Lett.* **2009**, *95*, 112105.
- [21] B. Hinnemann, P. G. Moses, J. Bonde, K. P. Jørgensen, J. H. Nielsen, S. Horch, I. Chorkendorff, J. K. Nørskov, *Chem. Soc.* **2005**, *127*, 5308.
- [22] H. D. Abruña, G. A. Hope, A. J. Bard, *J. Electrochem. Soc.* **1982**, *129*, 2224.
- [23] L. Britnell, R. M. Ribeiro, A. Eckmann, R. Jalil, B. D. Belle, A. Mishchenko, Y.-J. Kim, R. V. Gorbachev, T. Georgiou, S. V. Morozov, A. N. Grigorenko, A. K. Geim, C. Casiraghi, A. H. C. Neto, K. S. Novoselov, *Science* **2013**, *340*, 1311.
- [24] Q. H. Wang, K. Kalantar-Zadeh, A. Kis, J. N. Coleman, M. S. Strano, *Nat. Nanotechnol.* **2012**, *7*, 699712.
- [25] A. Ramasubramanian, *Phys. Rev. B* **2012**, *86*, 115409.
- [26] P. Tonndorf, R. Schmidt, P. Böttger, X. Zhang, J. Börner, A. Liebig, M. Albrecht, C. Kloc, O. Gordan, D. R. T. Zahn, S. Michaelis de Vasconcellos, R. Bratschitsch, *Opt. Express* **2013**, *21*, 49084916.
- [27] H. Fang, S. Chuang, T. C. Chang, K. Takei, T. Takahashi, A. Javey, *Nano Lett.* **2012**, *12*, 37883792.
- [28] H.-M. Li, D.-Y. Lee, M. S. Choi, D. Qu, X. Liu, C.-H. Ra, W. J. Yoo, *Sci. Rep.* **2014**, *4*, 4041.
- [29] S. Tongay, J. Zhou, C. Ataca, K. Lo, T. S. Matthews, J. Li, J. C. Grossman, J. Wu, *Nano Lett.* **2012**, *12*, 55765580.
- [30] Y. Zhao, W. Wang, C. Li, Y. Xu, L. He, *Solid State Commun.* **2018**, *281*, 0038.
- [31] F. S. Liu, J. X. Zheng, M. J. Huang, L. P. He, W. Q. Ao, F. Pan, J. Q. Li, *Sci. Rep.* **2014**, *4*, 5774.
- [32] G. Kresse, J. Hafner, *Phys. Rev. B* **1993**, *47*, 558.
- [33] G. Kresse, J. Furthmüller, *Comput. Mater. Sci.* **1996**, *6*, 15.
- [34] G. Kresse, J. Furthmüller, *Phys. Rev. B* **1996**, *54*, 11169.
- [35] G. Kresse, D. Joubert, *Phys. Rev. B* **1999**, *59*, 1758.
- [36] G. I. Csonka, J. P. Perdew, A. Ruzsinszky, P. H. T. Philipsen, S. Lebègue, J. Paier, O. A. Vydrov, J. G. Ángyán, *Phys. Rev. B* **2009**, *155*107.
- [37] J. P. Perdew, K. Burke, M. Ernzerhof, *Phys. Rev. Lett.* **1996**, *77*, 3865.
- [38] P. E. Blöchl, O. Jepsen, O. K. Andersen, *Phys. Rev. B* **1994**, *49*, 16223.
- [39] H. J. Monkhorst, J. D. Pack, *Phys. Rev. B* **1976**, *13*, 5188.
- [40] W. Tang, E. Sanville, G. Henkelman, *J. Phys.: Condens. Matter* **2009**, *21*, 084204.
- [41] E. Sanville, S. D. Kenny, R. Smith, G. Henkelman, *J. Comput. Chem.* **2007**, *28*, 899.
- [42] G. Henkelman, A. Arnaldsson, H. Jónsson, *Comput. Mater. Sci.* **2006**, *36*, 354.
- [43] M. Yu, D. R. Trinkle, *J. Chem. Phys.* **2011**, *134*, 064111.
- [44] G. K. H. Madsen, D. J. Singh, *Comput. Phys. Commun.* **2006**, *67*, 175.
- [45] T. J. Scheidemantel, C. Ambrosch-Draxl, T. Thonhauser, J. V. Badding, J. O. Sofo, *Phys. Rev. B* **2003**, *68*, 125210.
- [46] L. Jodin, J. Tobola, P. Pêcheur, H. Scherrer, S. Kaprzyk, *Phys. Rev. B* **2004**, *70*, 184207.
- [47] L. Chaput, P. Pêcheur, J. Tobola, H. Scherrer, *Phys. Rev. B* **2005**, *72*, 085126.
- [48] V. Wang, N. Xu, J. C. Liu, G. Tang et al., VASPKIT: A Pre- and Post-Processing Program for VASP Code, arXiv:1908.08269, **2019**.
- [49] M. E. Eanes, J. A. Ibers, *I-Kristallogr. NCS* **2001**, 216.
- [50] J. Ellermeier, C. Näther, W. Bensch, *Acta Crystallogr. C* **1999**, *55*, 1748.
- [51] C. C. Raymond, P. K. Dorhout, S. M. Miller, *Z. Kristallogr.* **1995**, *210*, 775.
- [52] A. Von Muller, W. Sievert, *Z. Anorg. Allg. Chem.* **1974**, *403*, 251.
- [53] M. T. Robinson, *J. Phys. Chem.* **1958**, *62*, 925.
- [54] H. Schäfer, G. Schäfer, A. Weiss, *Z. Naturforsch.* **1964**, *19b*, 76.
- [55] M. Born, K. Huang, *Dynamical Theory of Crystal Lattices*, Clarendon Press, Oxford **1956**, pp. 140–153.
- [56] W. Voigt, *Lehrbuch der Kristallphysik (mit Ausschluss der Kristalloptik)*, B. G. Teubner, Leipzig Berlin **1928**; Reprint edition: J. W. Edwards, Ann Arbor, MI, **1946**, pp. 1850–1919.
- [57] A. Reuss, *Z. Angew. Math. Mech.* **1929**, *9*, 49.
- [58] R. Hill, *Proc. Phys. Soc. Sect. A* **1965**, *65*, 349.
- [59] B. Lorenz, I. Orgzall, P. K. Dorhout, C. C. Raymond, H. D. Hochheimer, *Solid State Commun.* **1996**, *97*, 535.
- [60] X. Luo, B. Wang, *J. Appl. Phys.* **2008**, *104*, 073518.
- [61] V. K. Sharma, V. Kanchana, M. K. Gupta, R. Mittal, *J. Solid State Chem.* **2020**, *290*, 121541.
- [62] K. P. Ong, D. J. Singh, P. Wu, *Phys. Rev. Lett.* **2010**, *104*, 176601.
- [63] T. M. Tritt, M. A. Subramanian, *MRS Bull.* **2006**, *31*, 188.

- [64] V. K. Gudelli, V. Kanchana, G. Vaitheeswaran, *J. Phys.: Condens. Matter* **2015**, *28*, 025502.
- [65] P. C. Sreeparvathy, V. Kanchana, *J. Phys.: Condens. Matter* **2018**, *30*, 295501.
- [66] G. A. Slack, in *Solid State Physics: Advances in Research and Applications*, Vol. 34 (Eds: H. Ehrenreich, F. Seitz, D. Turnbull) Academic Press, New York **1979**, pp. 1–71.
- [67] Y. Zhang, *J. Materiomics* **2016**, *2*, 237.
- [68] D. T. Morelli, V. Jovicic, J. P. Heremans, *Phys. Rev. Lett.* **2008**, *101*, 035901.
- [69] E. J. Skoug, J. D. Cain, D. T. Morelli, *Appl. Phys. Lett.* **2010**, *96*, 181905.
- [70] Y. Zhang, E. Skoug, J. Cain, V. Ozoliņš, D. Morelli, C. Wolverton, *Phys. Rev. B* **2012**, *85*, 054306.
- [71] J. M. Ziman, in *Electrons and Phonons: The Theory of Transport Phenomena in Solids* (Eds: N. F. Mott, B. C. Bullard, D. H. Wilkinson), Oxford University Press, Oxford, UK **1960**, pp. 128–156.
- [72] C. Kittel, *Introduction to Solid State Physics*, 8th ed., John Wiley & Sons, Inc., New York, NY **1986**, pp. 121–124.
- [73] D. G. Cahill, S. K. Watson, R. O. Pohl, *Phys. Rev. B* **1992**, *46*, 6131.
- [74] T. Jia, G. Chen, Y. Zhang, *Phys. Rev. B* **2017**, *95*, 155206.
- [75] G. A. Slack, *J. Phys. Chem. Solids* **1973**, *34*, 321.
- [76] N. A. Noor, M. Rashid, Q. Mahmood, B. Ul Haq, M. A. Naeem, A. Laref, *Opto-Electron. Rev.* **2019**, *27*, 194201.
- [77] M. Dadsetani, A. Pourghazi, *Phys. Rev. B* **2006**, *73*, 195102.
- [78] N. V. Smith, *Phys. Rev. B* **1971**, *3*, 1862.
- [79] P. C. Martin, *Phys. Rev. B* **1967**, *161*, 143.
- [80] S. A. Abbas, I. Mahmood, M. Sajjad, N. A. Noor, Q. Mahmood, M. A. Naeem, A. Mahmood, S. M. Ramay, *Chem. Phys.* **2020**, *538*, 110902.